WPMST1-PR(18) 19899

P. Manz et al.

On the phase velocity in between weak and strong plasma edge turbulence

Preprint of Paper to be submitted for publication in
Plasma Physics and Controlled Fusion

This work has been carried out within the framework of the EUROfusion Consortium and has received funding from the Euratom research and training programme 2014-2018 under grant agreement No 633053. The views and opinions expressed herein do not necessarily reflect those of the European Commission.

On the phase velocity in between weak and strong plasma edge turbulence

P. Manz[1], D. Prisiazhniuk[1], T. Happel[1], S. Freethy[1], K. Hallatschek[1], B.D. Scott[1], U.Stroth[1,2] and the ASDEX Upgrade Team
[1] *Max-Planck-Institut für Plasmaphysik, Boltzmannstr.2 ,85748 Garching, Germany*
[2] *Physik-Department E28, Technische Universität München, James-Franck-Str. 1, 85748 Garching, Germany*
(Dated: February 23, 2018)

In the case of strong edge turbulence linear features as growth rates and dispersion can be suppressed by small-scale vorticity generated by nonlinear self-sustainment. Measurements by different diagnostic techniques could still provide finite values. The phase velocity measured by a frequency dependent technique will be always in the same direction as the background velocity, where a wavenumber dependent technique measures a phase velocity in the opposite direction. These phase velocities are a result of the nonlinear redistribution of spectral energy and not a result of the linear instabilities. It is recommended to verify phase velocity measurements based on a frequency dependent technique with a wavenumber dependent technique and vice versa.

PACS numbers:

I. INTRODUCTION

The edge of magnetized confined plasmas is subject to a wide number of different modes resulting from varying linear instabilities and diverse nonlinear self-organized phenomena. It is widely thought that an underlying instability grows and excites the turbulence by nonlinear saturation [1]. During such a process various features of the underlying instability may be transmitted to the turbulence [2–4]. Different modes or instabilities can be distinguished by their size, cross-phase relations between different quantities (as density, potential, electron and ion temperature and heat fluctuations) and their dispersion relation between wavenumber k and frequency ω. An overview of the propagation direction, cross-phases and typical sizes of the most relevant instabilities for the plasma edge can be found in [5]. As cross-phase relations are commonly not available in the experiment, the phase velocity is usually one of the key identifiers for the underlying instability. At low fluctuation level typically observed in the plasma core this may be a proper treatment. On the other hand at high fluctuation levels, characteristic for the low confinement regime in the plasma edge, drift waves can nonlinearly sustain themselves and linear instabilities can be fairly irrelevant [6, 7]. This is the reason why turbulence in the plasma edge in the low confinement regime is expected to be drift-wave dominated [8]. The dispersion relation of drift waves is given by

$$\omega_l = \frac{u_{e,dia} k_y}{1 + (\rho_s k_\perp)^2}. \quad (1)$$

The index l in the frequency ω_l is specified to distinguish the linear frequency from the nonlinear frequency later. Drift waves exhibit a phase velocity ω_l/k close to the electron diamagentic velocity $u_{e,dia}$ and propagate binormal ($k = \mathbf{k}_y$) to the parallel magnetic field and radial direction ($\mathbf{k}_x$). The perpendicular plane is spanned by the radial and binormal direction ($\mathbf{k}_\perp = \mathbf{k}_y + \mathbf{k}_x$). Due to polarization effects the phase velocity is reduced by $(\rho_s k_\perp)^2$ at structures close to the drift-scale $\rho_s = \sqrt{T_e m_i}/(eB)$, with elementary charge e, magnetic field strength B, ion mass m_i and electron temperature T_e.

Measurements in ASDEX Upgrade with Doppler reflectometry show no significant phase velocity in the plasma edge and the measured velocity is approximately the $E \times B$ background velocity [9] showing also no signs of dispersion [10]. This has been also observed in W7-AS [11]. This seems to be in contradiction to drift-waves being the dominant instability in the plasma edge from a linear perspective. On the other hand finite phase velocities have been reported from the plasma core in ASDEX Upgrade [12, 13] and between plasma core and edge in Tore Supra [14].

For the purpose of illustration an example of measurements at different wavenumbers is shown in Fig. 1. The data is shown in normalized dimensionless units (left hand side and bottom) and in dimension-assigned units (right hand side and top). The Doppler reflectometer (DR) with a movable mirror allows probed varying wavenumbers ($6 < k_\perp < 12$ cm^{-1}) during the discharge, the poloidal correlation reflectometer (PCR) [10] is sensitive at low wavenumbers ($k_\perp < 3$ cm^{-1}). The measured Doppler frequency shows a linear relationship to the probed wavenumber (Fig. 1a). The measured frequency by the PCR aligns well with the one by DR. The $E \times B$ background velocity has been estimated by $u_{E\times B} \approx (1/en)\nabla p_i \approx (1/en)\nabla p_e$ to be around 4 km/s (indicated by the blue shaded area in Fig. 1), the measured dispersion in the phase velocity is small (< 0.35 km/s) and is within the error bars of the measurements. A possible phase velocity is significantly below the electron diamagnetic velocity which is of the order of $u_{E\times B}$ as indicated by the black shaded line in Fig. 1.

In the following, turbulence will be classified in weak and strong turbulence regimes (Sec. I B). With the help of simulations (details given in Sec. II) the influence of the strength of broadband turbulence on the measure-

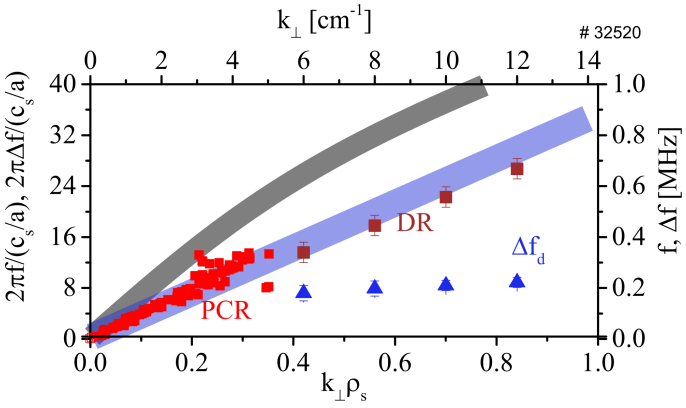

FIG. 1: Frequency versus wavenumber measured at the plasma edge ($\rho_{pol} = 0.985$) of a typical ASDEX Upgrade L-mode plasma at a temperature of $T_e = 124$ eV, the frequency is normalized to the cold ion sound speed c_s, the wavenumber to $\rho_s = 0.7$ mm calculated with the magnetic field on axis $B = 2.6$ T. The frequency broadening Δf (blue) is about 1/3 of the measured frequency. The corresponding perpendicular velocity $\partial f/\partial k$ is not varying with the wavenumber within the error bars. The estimate for the $E \times B$ velocity is indicated by the blue shaded area, an estimate of the drift-wave dispersion relation is indicated by the black shaded area.

ments of a phase velocity will be investigated. Different measurement techniques to determine the phase velocity will be discussed in Sec. I A. These are studied in a simulated case of weak turbulence (Sec. III), strong turbulence (Sec. V) and in a regime between weak and strong turbulence corresponding to the experimental situation (Sec.IV). It will be shown that the high fluctuation level of the turbulence (in particular the high level of vorticity fluctuations) in the plasma edge is strong enough to suppress linear features of the plasma turbulence. Measured finite phase velocities can be a result of the turbulent cascade independent of an underlying instability. Summary and conclusions are given in Sec. VI.

A. Measured dispersion in dependence of the measurement technique

To infer spatial characteristics from temporal signals, experimentally one have to map time to space mainly motivated by Taylor's hypothesis of frozen turbulence [15]. It is assumed that at a point the change of turbulent velocity fluctuations in time can be directly related to their spatial change via the mean convection velocity. Already in the fifties it was shown that the hypothesis breaks down and is restricted to a limited range of wavenumbers (or frequencies) for shear flows [16]. The applicability of Taylor's hypothesis also depends on the fluctuation level, to be valid turbulent velocity fluctuations must be significant smaller than the mean velocity [16]. Due to the power distribution in the wavenumber-frequency plane $P(k,\omega)$, the power of a single frequency will have contributions from multiple wavenumbers. This can result in a difference between two ways of determining average wave velocities given by the direction of integration. One can integrate in wavenumber direction keeping frequency constant or integrate in frequency direction and keep wavenumber constant. Depending on the shape and the broadening of the wavenumber-frequency distribution, this results in different answers as we will see in the following.

For example by choosing the wavenumber to be constant, k_0, we take a cut in the frequency direction. The average frequency is defined by

$$\langle\omega\rangle(k_0) = \frac{\int P(k_0,\omega)\omega d\omega}{\int P(k_0,\omega)d\omega}. \tag{2}$$

Doppler reflectometry measures a power spectrum $P(k_0,\omega)$ at a given wavenumber k_0, from which a wavenumber dependent phase velocity $u(k_0) = \frac{\langle\omega\rangle(k_0)}{k_0}$ can be estimated in principle. Since the low frequency range is often corrupted by the directly reflected microwave beam this analysis approach is often misleading and the Doppler shift should be determined by fitting a Gaussian to the power spectrum.

By choosing a constant frequency ω_0 to examine wave velocities, cuts along the wavenumber direction in $P(k,\omega_0)$ give an average wavenumber defined by

$$\langle k\rangle(\omega_0) = \frac{\int P(k,\omega_0)kdk}{\int P(k,\omega_0)dk}. \tag{3}$$

A wave velocity can be estimated by $u(\omega_0) = \frac{\omega_0}{\langle k\rangle}$. Measuring a wavenumber by estimating it by the phase difference of spatially separated points leads to such estimates. If fluctuations can be represented by an eikonal $\sim \exp(i\theta)$ with $\theta = kx - \omega t$ the effective or pseudo wavenumber [17] is given by $\langle k\rangle(\omega) = \frac{\partial\theta}{\partial x}$. Mode numbers of magnetic signals are usually estimated in this way [18]. Time delay estimation (TDE) works in a similar manner. Also here the phase is measured at two spatially displaced positions $\theta(x,t)$ and $\theta(x+\Delta x,t)$. Now the time lag Δt is estimated, where both signals are in phase. Hence, $\theta(x,t) = \theta(x+\Delta x, t+\Delta t)$ or $k\Delta x = \omega\Delta t$. From this a frequency dependent phase velocity can be directly inferred $u_{ph}(\omega) = \frac{\omega}{k} = \frac{\Delta x}{\Delta t}$. The spatial displacement Δx, a time delay Δt and the frequency at which the time delay is measured are determined. Actually also here an effective phase velocity $\langle u\rangle_{TDE}(\omega) = \frac{\omega}{\langle k\rangle_{TDE}}$ or an effective wavenumber $\langle k\rangle_{TDE}(\omega) = \frac{\omega}{\Delta x}\Delta t$ are estimated. There are additional problems like propagation into the radial direction or eddy tilting which can be diminished by taking into account multiple spatial points, but also TDE methods including multiple spatial points [19–21] or velocimetry [22] relies basically on the same assumptions. However, if the measured field contains all important spatial scales of motion it should be in principle appropriate to the recover the phase velocity. Nearly all

measurements of velocities done with Langmuir probe arrays, gas-puff or electron-cyclotron emission imaging, beam emission spectroscopy, correlation reflectometry, phase contrast imaging measure an effective wavenumber $\langle k \rangle(\omega)$.

In this study these two different measurement methods of estimation of phase velocities are investigated in the case between weak and strong plasma edge turbulence.

B. Turbulence regimes

The distinction between weak and strong turbulence goes back to Kadomtsev [1] and the latest review can be found in Ref. [23]. The regimes of turbulence are distinguished by the strength of fluctuations represented by spectral broadening. The frequency broadening is defined by

$$\Delta\omega(k) = \sqrt{\frac{\int P(k,\omega)\omega^2 d\omega}{\int P(k,\omega) d\omega} - \langle\omega\rangle^2}. \quad (4)$$

The wavenumber broadening is defined by

$$\Delta k(\omega) = \sqrt{\frac{\int P(k,\omega)k^2 dk}{\int P(k,\omega) dk} - \langle k\rangle^2}. \quad (5)$$

In the picture of weak turbulence a wave-like instability grows and its nonlinear saturation is responsible for the turbulence. To retain its wave-like features the frequency is similar to the linear eigenfrequency $\langle\omega\rangle \sim \omega_l$ and the growth rate is smaller than the linear eigenfrequency $\gamma_l \ll \omega_l$. The weak turbulence regime is also called wave turbulence. The growth rate of the instability is balanced by nonlinear saturation $\gamma_l \sim \Delta\omega$. Weak turbulence is characterized by small frequency broadening $\Delta\omega \ll \omega_l$.

In the strong turbulence regime the nonlinearities dominate and the turbulence is independent of the excitation process. Strong turbulence is characterized by strong frequency broadening $\Delta\omega$ exceeding the analytically expected eigenfrequency $\Delta\omega \gg \omega_l$. As a result strong turbulence does not feature a linear wave frequency due to the short decorrelation time $\tau \approx 1/\Delta\omega$ resulting in $\gamma_l \ll \Delta\omega$, $\omega_l \ll \Delta\omega$. Equivalent considerations are valid for the wavenumber.

That the nonlinearity is not dominant in the weak turbulence case does not mean that it does not lead to a redistribution of spectral energy and cascades are not present. It just means that the turbulent spectral power $P(k,\omega)$ is tightly bound to the linear dispersion relation in the wavenumber-frequency plane as indicated by the grey region in Fig. 2a. Along the dispersion relation the spectral power can be redistributed and a cascade can be observed as indicated by the blue upper spectrum in Fig. 2a. However, vertical and horizontal cuts through the wavenumber-frequency plane, corresponding to frequency (wavenumber) spectra at a given wavenumber

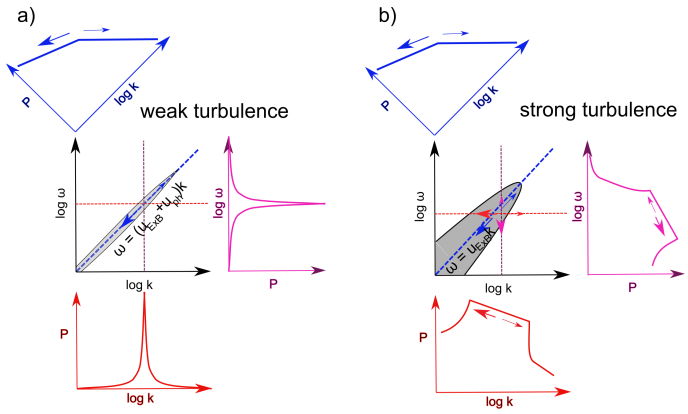

FIG. 2: Artist's view of spectral features of weak and strong turbulence.

(frequency), show no cascades and just the dispersion. In the case of strong turbulence (Fig. 2b) the dispersion relation can be neglected and the spectral power mainly follows the Doppler shift of the background flow. Due to the strong nonlinearity the spectral power spreads in all directions with the tendency to lower frequencies and wavenumbers in the two-dimensional case. These can be also observed in the frequency (wavenumber) spectra at a given wavenumber (frequency).

II. SIMULATION SET UP

Simulations of circular plasma cross-section with toroidal axisymmetry have been carried out with the three-dimensional gyrofluid electromagnetic turbulence model GEMR [24, 25]. GEMR simulates the densities, parallel velocities, parallel and perpendicular temperatures and parallel and perpendicular parallel heat fluxes for ions and electrons, respectively. The coordinate system is aligned with the equilibrium magnetic field. Although being a δ-f limited code the gradients evolve freely and GEMR is a global model. Details on the self-consistent treatment of the profiles and MHD equilibrium can be found in Ref. [24]. The main input paramters of GEMR are a smallness parameter $\delta = \rho_s/a$, a normalized plasma beta β and a normalized collisionality $\nu = a\nu_e/c_s$ with ν_e the inverse Braginskii electron collision time. Simulations have been carried out at ASDEX Upgrade parameters ($R = 1.65$ m, $a = 0.5$ m, $B = 2.4$ T, $q_s = 4.6$). The coordinate system (x, y, s) is in the radial, binormal and parallel direction to the magnetic field. The simulations are performed on a $128 \times 512 \times 16$ grid, where only the drift plane (128×512) at the outboard midplane is analyzed here. The simulations cover the region $0.96 < \rho < 1.04$.

Typical experimental parameters at the last closed flux surface (LCFS) as the reference flux surface are chosen. The case corresponding to the experimental situation

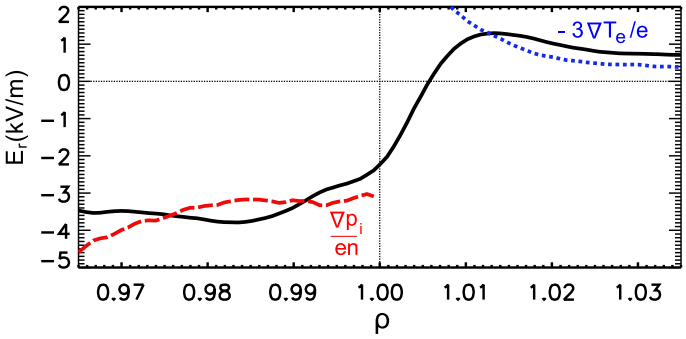

FIG. 3: Strong turbulence case: Radial electric field (black solid line), ion pressure contribution (red dashed line) and sheath potential (blue dotted line) to the radial electric field.

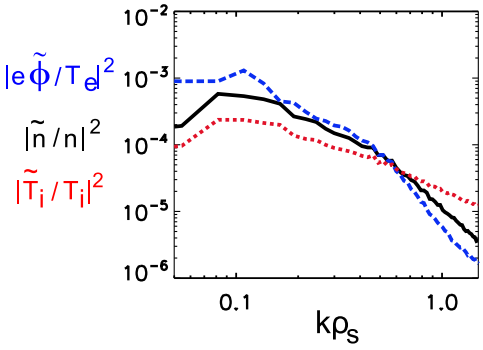

FIG. 4: Strong turbulence case: Wavenumber spectra of normalized potential (blue), density (black) and ion temperature (red) fluctuations. At low wavenumbers potential perturbations are strongest corresponding to ballooning modes, at higher wavenumbers density and potential fluctuations are similar and the ion temperature fluctuations are strongest pointing to ITG-drift-wave turbulence.

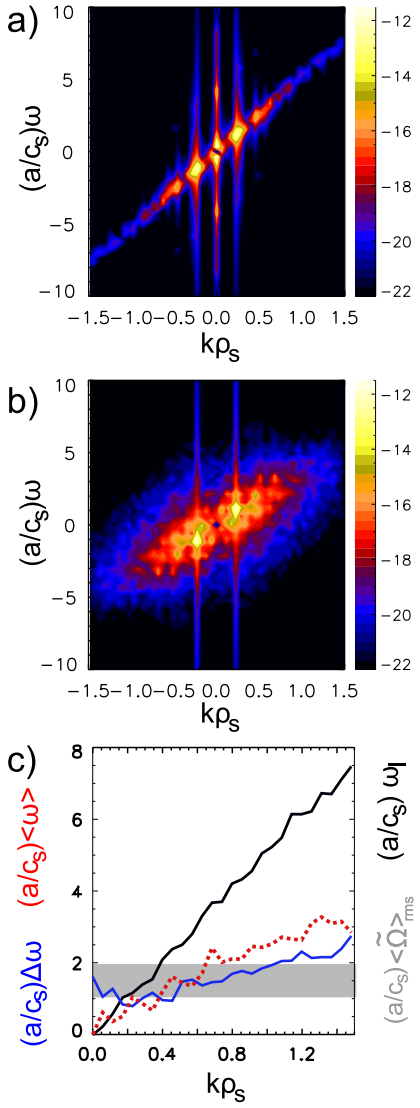

FIG. 5: Weak turbulence case: Wavenumber-frequency power spectrum $P(k,\omega)$ of density fluctuations at $\rho = 0.5$ in the plasma frame in the late growth phase (a) and in the saturated phase (b). Frequency broadening shown by the blue solid line compared to the average frequency in the plasma frame shown by black solid (red dotted line) in the growth (saturated) phase, respectively (c). The rms vorticity level is indicated by the gray area. The linear eigenfrequency (black line) exceeds both the frequency broadening and rms vorticity level.

(Sec. IV) is at $n_e = 2\cdot10^{19}$ m^{-3}, $T_e = T_i = 120$ eV corresponding to $\delta = 1.32\cdot10^{-3}$, $\beta = 8.39\cdot10^{-5}$ and $\nu = 4.08$. The gradient scale lengths are fixed and not allowed to evolve, chosen to be $L_n = 0.5L_{Te} = 0.5L_{Ti} = 2.5$ cm as in the experimental situation. The strong turbulence case (Sec. V) is at $n_e = 2\cdot10^{19}$ m^{-3}, $T_e = T_i = 100$ eV corresponding to $\delta = 1.20\cdot10^{-3}$, $\beta = 6.99\cdot10^{-5}$ and $\nu = 5.88$. Initial gradient scale lengths have been chosen to be $L_n = 0.5L_{Te} = 0.5L_{Ti}$. All simulations have been done on a $128\times512\times16$ grid. The radial resolution is 0.65 ρ_s, the resolution of the binormal plane is 0.55 ρ_s. Under these conditions we expect drift-wave turbulence [8].

In the strong turbulence case (Sec. V) the gradients evolve. During the initial phase the density gradient relaxes and the ion temperature gradient effectively steepens up compared to the density gradient $L_n = (2/3)L_{Ti} = 5$ cm. The radial electric field is shown in Fig. 3, it is dominated by its ion pressure contribution in the confined region and by the sheath potential in the scrape-off layer. Depending on the wavenumber the turbulence shows different features. At low wavenumbers ($k\rho_s < 0.2$) potential perturbations are strongest corresponding to resistive ballooning modes (see Fig. 4). At higher wavenumbers ($k\rho_s > 0.2$) density and potential fluctuation amplitudes are similar which is characteristic for drift-wave turbulence. At even higher wavenumbers ($k\rho_s > 0.6$) the ion temperature fluctuations are strongest pointing to ITG-drift-wave turbulence.

For the sake of completeness also a weak turbulence case is presented in Sec. III. Weak turbulence can be obtained for small gradients appearing for example in the core. The reference surface has been chosen to be at $\rho = 0.5$ with $n_e = 4.5 \cdot 10^{19}$ m^{-3}, $T_e = T_i = 2$ keV. The cover the region $0.3 < \rho < 0.7$ with a gradient scale lengths of $L_{Ti} = L_{Te} = 0.3 L_n = 20$ cm. In such a case ITG turbulence can be expected. The corresponding GEMR input parameters are $\delta = 5.38 \cdot 10^{-3}$, $\beta = 3.15 \cdot 10^{-3}$ and $\nu = 0.03$. The results are shown in the following section III.

III. MARGINAL WEAK TURBULENCE REGIME $\Delta\omega < \omega_l$

For the purpose of introduction we start to study a weak turbulence case. The wavenumber-frequency power spectrum $P(k, \omega)$ of density fluctuations in the plasma frame of reference at $\rho = 0.5$ are shown in Fig. 5a in the late growth phase of the simulation. The directions are defined positive for ion diamagnetic direction and negative in the electron diamagnetic direction. As ω/k is positive a clear phase velocity in ion diamagnetic direction can be observed, which is a signature of ITG turbulence. From Eq. (2) the linear phase velocity can be measured, which is shown by the black line in Fig. 5c. Most of the turbulence activity is restricted to this very narrow line. This situation corresponds to the weak turbulence case, beside it is not saturated yet. The turbulence saturates to a fluctuation level of about $\tilde{n}/n \approx 1\%$. In the saturated phase the turbulence gets more broadband as shown by Fig. 5b. The averaged frequency $\langle\omega\rangle$ as shown by the red dotted line in Fig. 5c is reduced compared to the growth phase, but a phase velocity in ion diamagnetic direction is clearly observable. The averaged frequency $\langle\omega\rangle$ is above the frequency broadening $\langle\omega\rangle > \Delta\omega$ (shown by the blue line in Fig. 5c). Therefore, this case is in the weak turbulence regime even though not ideal as the frequency does not exceed the broadening much. With respect to the linear frequency (shown by the black line in Fig. 5c) the turbulence is in the weak turbulence regime. The underlying instability (ITG) can imprint its linear phase velocity to the turbulence. The linear frequency significantly exceeds the frequency broadening $\omega_l \sim \langle\omega\rangle \gg \Delta\omega$ and rms vorticity (that will be important later, indicated by the gray region in Fig. 5c).

IV. MARGINAL STRONG TURBULENCE REGIME $\Delta\omega \gtrsim \omega_l$

In the experimental situation in ASDEX Upgrade usually a significant frequency broadening is present, however, it does not exceed the averaged frequency. In Fig. 1 the frequency broadening as estimated from the Doppler reflectometry is $\Delta f_{meas}/\langle f_{meas}\rangle \approx 0.3$. Therefore typical L-mode plasmas at the plasma edge in ASDEX Upgrade are closer to a weak turbulence regime. Due to the turbulence the frequency is broadened by $\Delta\omega(k) = k\Delta u + u_{E\times B}\Delta k + \Delta k \Delta u$, where Δk is the nonlinear wavenumber broadening and Δu is the nonlinear broadening or the velocity spectrum. The measured frequency broadening is not only due to fluctuations at the probing wavenumber k_0 but also due to the finite spectral resolution Δk_0 probed [26, 27], resulting in a frequency broadening $2\pi\Delta f_{diag} = \Delta k_0 \cdot u$. Taking $\Delta k_0 = 2.2$ cm^{-1} cm we get $\Delta f_{diag}/\Delta f_{meas} \approx 0.5$. As Δf_{diag} gives basically the sensitivity of the diagnostics it is likely that Δf_{meas} provides the correct estimate of the frequency broadening by the turbulence. At least it is not higher $\Delta\omega < 2\pi\Delta f_{meas}$. In a conservative approach the minimum frequency broadening by the turbulence would be $\Delta\omega > 2\pi(\Delta f_{meas} - \Delta f_{diag})$, therefore $\Delta\omega/\langle\omega\rangle \approx 0.15$–

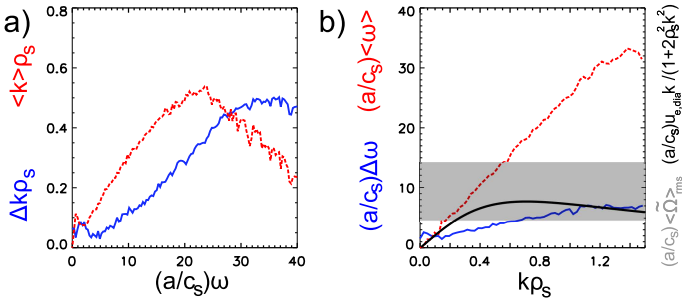

FIG. 6: Marginal strong turbulence case: Wavenumber (a) and frequency (b) broadening shown by blue solid lines compared to the average wavenumber and frequency shown by red dashed lines. Also the drift-wave eigenfrequency is shown included as a black line and the rms vorticity level is indicated by the grey area. Data is shown in the laboratory frame of reference.

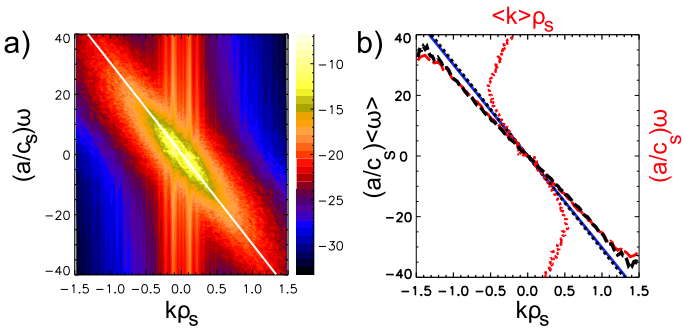

FIG. 7: Marginal strong turbulence case: Wavenumber-frequency power spectrum $P(k, \omega)$ of density fluctuations at $\rho = 0.980$ (a), the mode at $k\rho_s = 0.1$ is an interchange mode. Frequency averaged frequency $\langle\omega\rangle(k)$ (red dashed line), the mean $E \times B$ velocity $\omega = u_{E\times B}k$ (blue solid line), phase velocity by wavenumber average $\omega/\langle k\rangle$ (red dotted line), fitted mean of the Gaussian in dependence of wavenumber (black dashed line) and measured phase velocity by TDE (black dotted line) (b). Data is shown in the laboratory frame of reference.

0.3.

A weak turbulence regime in the plasma edge seems not to be easily accessible in GEMR. By fixing the background profiles to the initial conditions a reduction in the spectral broadening can be obtained. Beside at very low frequencies the averaged frequency strongly exceeds the frequency broadening $\langle\omega\rangle(k) \gg \Delta\omega(k)$ (Fig. 6b) by $\langle\omega\rangle(k)/\Delta\omega(k) \approx 4 - -7$. This is of a similar order as in the experimental observation (Fig. 1) where the averaged frequency exceeds the frequency broadening by $\langle\omega\rangle(k)/\Delta\omega(k) \approx 1.5 - -3.5$ (taking into account broadening by diagnostic effects discussed above this factor maybe assumed to be$\langle\omega\rangle(k)/\Delta\omega(k) \approx 3 - -7$). At these low frequencies an interchange instability is present. As seen in Fig. 7b $\langle\omega\rangle(k) \approx u_{E\times B}k$ and no significant wavenumber shift is observed. Approximating velocities by the center of gravity of the frequency [28] as done by Eq. (2) is not the usual evaluation method. Commonly a Gaussian is fitted to the logarithmic power spectrum $P(k_0, \omega)$. The center of the Gaussian is equalized to the Doppler shift as the advection velocity. Also using such procedure the background velocity is recovered. The averaged wavenumber $\langle k\rangle(\omega)$ strongly exceeds the wavenumber broadening $\Delta k(\omega)$ up to roughly $(a/c_s)\omega < 20$ (Fig. 6a). For low frequencies with low frequency broadening ($(a/c_s)\omega < 20$) the phase velocity follows the background velocity only $\omega/\langle k\rangle \approx u_{E\times B}k$ (Fig. 7b). At higher frequencies with significant broadening in wavenumber space (Fig. 6a) a propagation in electron diamagnetic direction is observed (Fig. 7b). However, this shift is mainly due to the presence of an interchange mode at $k\rho_s \approx 0.1$ (Fig. 7a). Also note that the measurements in ASDEX Upgrade do not cover this region. Also a frequency dependent diagnostic will usually not evaluate Eq. (3), but instead estimate the velocity by correlation. Indeed the velocity estimated with TDE using a spatial separation of about 5 mm (black dotted line in Fig. 7b) recovers the background velocity (blue solid line in Fig. 7b) as shown by the overlap of the lines in Fig. 7b). In summary, this simulation does not show any significant phase velocity in the plasma frame nor dispersion.

How linear features can get lost in drift-wave turbulence can be found in Ref. [29], which is shortly summarized here. In the weak turbulence picture the linear growth rate balances the nonlinear broadening $\gamma_l \sim \Delta\omega$. This is not the case for fully developed drift-wave turbulence in the plasma edge; the linear growth rate is much smaller than the rms vorticity $\gamma_l \ll \langle\tilde{\Omega}\rangle_{rms}$ [29]. As the nonlinear spectral transfer is done mainly by the vorticity equation, the rms vorticity should be of the order of the frequency broadening $\langle\tilde{\Omega}\rangle_{rms} \sim \Delta\omega$. Regarding the aspect $\gamma \sim \Delta\omega$ fully developed drift-wave turbulence is not in the weak turbulence regime [29].

At the beginning of the simulation the transition to turbulence occurs and the growth phase can be studied. Below $t < 30\ c_s/a$ the turbulence is exponentially growing as seen by the amplitude in Fig. 8a. The growth

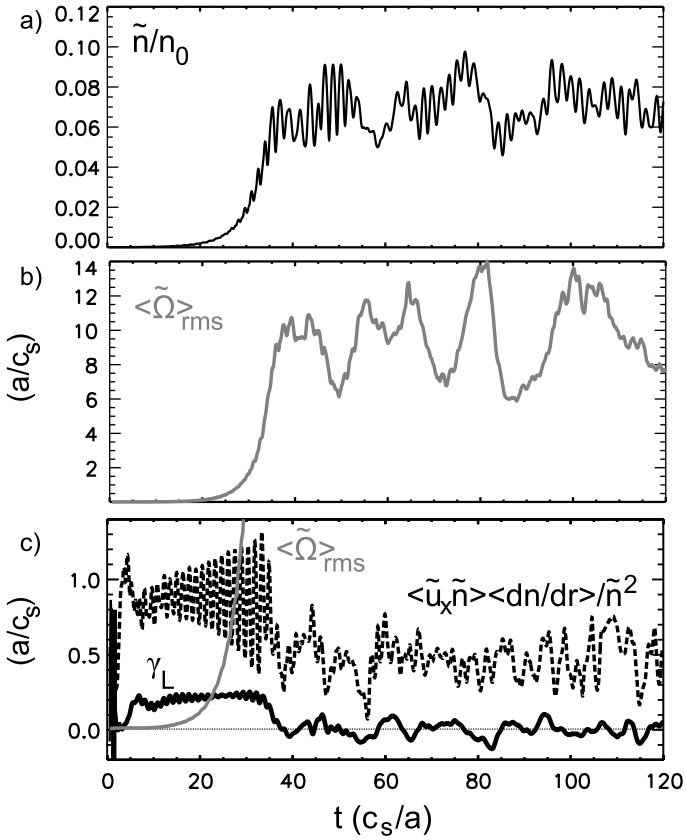

FIG. 8: Marginal strong turbulence case: Density fluctuation level (a), vorticity fluctuation level (b), vorticty, growth rate γ_l, turbulence gradient drive rate (c) at the beginning of the simulation.

rate is about $\gamma_l \approx 0.2\ c_s/a$ and is carried mainly by an interchange mode at $k\rho_s \approx 0.1$. As the density fluctuation level increases also the rms vorticity level increases. The vorticity is calculated by $\tilde{\Omega} = \nabla^2_\perp(\tilde{\phi} + \tilde{p}_i)$ and takes electrostatic potential and ion pressure fluctuations into account. At $t \approx 25\ c_s/a$ the rms vorticity exceeds the linear growth rate. Shortly after this at ($t \approx 35\ c_s/a$) the growth rate drops to zero. Also the turbulence gradient drive rate $\langle\tilde{u}_x\tilde{n}\rangle\langle dn/dr\rangle/\tilde{n}^2$ drops strongly. The turbulence level saturates. The turbulence has to generate its own vorticity through nonlinear self-sustainment [6, 7]. Similar to a background shear the nonlinear vorticity scatters small-structures apart before they can feel a linear instability. As a consequence linear features as the linear growth rate or propagation velocity can get lost. The growth rate $\gamma_l \approx 0.2\ c_s/a$ is much below $\langle\Omega\rangle_{rms}$ at 6–14 a/c_s, the vorticity rms level of the electrostatic potential fluctuations only is between 3–6 a/c_s. As the drift wave phase velocity is much higher than the growth rate $\omega_l \gg \gamma_l$ it might survive. In Fig. 6b the black line shows the drift-wave dispersion relation $\omega_l = u_{e,dia}k_y/(1 + \rho_s^2(k_x + k_y)^2)$ (see Eq. (1)) is approximated by $u_{e,dia}k/(1 + 2\rho_s^2k^2)$ assuming isotropic struc-

tures $k_x = k_y$. The drift-wave eigenfrequency is in a similar order of magnitude as the spectral broadening $\omega_l \approx \Delta\omega$ (blue line in Fig. 6b). Note one should compare not the eigenfrequency $\omega_l(k_l)$ at a particular scale with its spectral broadening $\Delta\omega(k_l)$ only, since the drift wave $\omega_l(k_l)$ is disturbed by the scales different to itself $k \neq k_l$. The total rms vorticity level $\tilde{\Omega}$ indicated by the gray shaded area in Fig. 6b) is at least similar to the linear eigenfrequency and mostly exceeds it (black line in Fig. 6b) which seems to be sufficient to mix and disturb the drift wave during its propagation and no typical drift-wave phase velocity is measured. The results confirm that the small-scale vorticity is generated at a rate similar to the diamagnetic drift frequency [7]. The structures are only advected by the background flow. The present regime shows features of strong turbulence $\gamma_l \ll \Delta\omega$, but as the eigenfrequency is close to the frequency broadening $\omega_l \gg \Delta\omega$ is not fulfilled. Therefore, the presented regime is closer to strong than to weak turbulence.

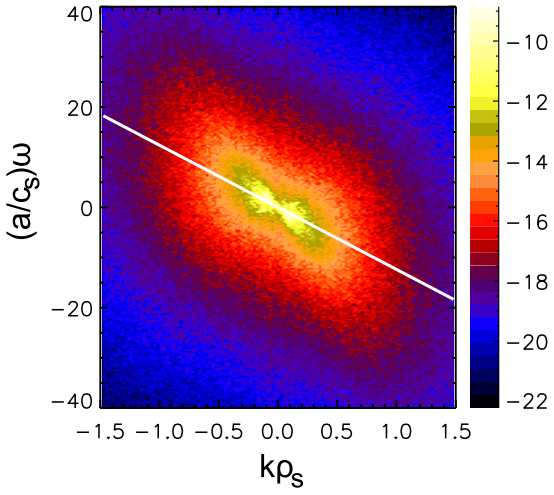

FIG. 10: Strong turbulence case: Wavenumber-frequency power spectrum $P(k,\omega)$ of density fluctuations at $\rho = 0.995$. Data is shown in the laboratory frame of reference.

V. STRONG TURBULENCE REGIME $\Delta\omega \gg \omega_l$

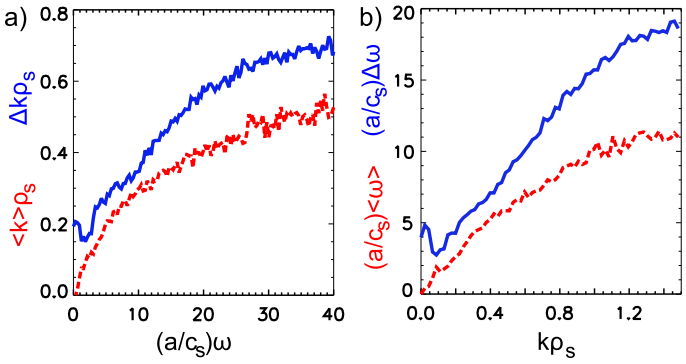

FIG. 9: Strong turbulence case: Wavenumber (a) and frequency (b) broadening shown by blue solid lines compared to the average wavenumber and frequency shown by red dashed lines. The broadening exceeds the averaged values but is of the same order of magnitude. Data is shown in the laboratory frame of reference.

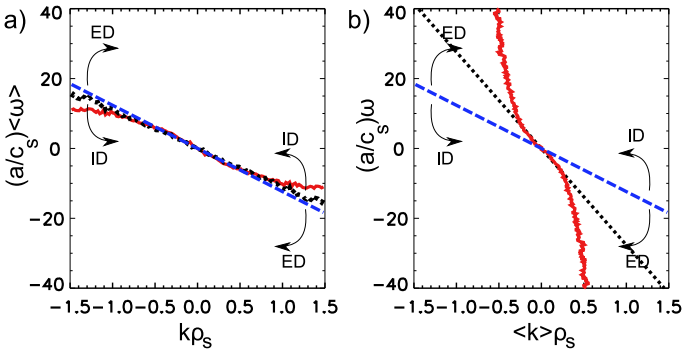

FIG. 11: Strong turbulence case: Averaged frequency $\langle\omega\rangle$ in dependence of the wavenumber (a) and averaged wavenumber $\langle k\rangle$ in dependence of the frequency ω (b) (both red solid lines) in comparison with the mean convective velocity $\omega = u_{E\times B}k$ (blue dashed line) in electron diamagnetic direction. The phase velocities in the plasma frame are indicated by the arrows. The l.h.s. shows a phase velocity in ion diamagnetic direction, the r.h.s. shows a phase velocity in electron diamagnetic direction. The measured velocity as measured by a Doppler is included by the dotted black line in (a), the measured velocity as measured by a TDE technique is included as a black dotted line in (b). Data is shown in the laboratory frame of reference.

In these simulations the spectral broadening exceeds the averaged value for both the frequency and wavenumber (Fig. 9). As the broadening does not exceed the averaged values by orders of magnitude ($\Delta\omega/\langle\omega\rangle \approx \frac{3}{2}$, $\Delta k/\langle k\rangle \approx \frac{4}{3}$) the simulations seem to be marginal in the strong turbulence regime.

A typical wavenumber-frequency spectrum of density fluctuations of the drift plane at the outboard midplane is shown in Fig. 10. The power distribution follows more or less the mean convective velocity as indicated by the white solid line $\omega = u_{E\times B}k$. The mean convective velocity is in electron diamagnetic direction, which is here defined negative. In Fig. 10 it appears like the turbulence amplitude is symmetrically spread around $\omega = u_{E\times B}k$.

By integrating in frequency space to estimate the mean frequency (Eq. (2)) a propagation in ion diamagnetic direction in the plasma frame is observed (see Fig. 11a). This is expected for ITG-modes. However, if we integrate in wavenumber space to estimate the mean wavenumber (Eq. (3)) and plot the frequency above this averaged wavenumber, modes at higher wavenumber propagate in electron diamagentic direction in the plasma frame (Fig. 11b), which is characteristic for drift waves. Indeed estimating the velocity by TDE using a spatial displace-

ment of 5 mm results in the phase velocity as shown by the black dotted line in Fig. 11b which is roughly two times the background $E \times B$ velocity. As the $E \times B$ velocity is roughly the ion diamagnetic velocity in electron diamagnetic direction the corresponding phase velocity as measured by TDE is the electron diamagnetic velocity as expected for electrostatic drift waves.

In summary, the structures propagate in ion diamagnetic direction at a given wavenumber and in electron diamagetic direction at a given frequency. In a linear framework this seems impossible.

The reason of the discrepancy of different phase velocities $\langle\omega\rangle/k$ and $\omega/\langle k\rangle$ is the nonlinear broadening. In the case of drift-wave turbulence the power is transferred to low frequencies and low wavenumbers [30–33] leading to the power being skewed to low wavenumbers and low frequencies. This is called the inverse energy cascade [34]. At a given wavenumber k the power is transferred to low frequencies responsible for a reduction of the effective frequency $\langle\omega\rangle$ and therefore also propagation velocity $\langle\omega\rangle/k$ compared to the background velocity. As in this example the background velocity is in the electron diamagnetic direction this leads to a propagation in ion diamagnetic direction in the plasma frame. At a given frequency ω the power is transferred to lower wavenumbers. This leads to a reduction of the effective wavenumber $\langle k\rangle$ at this frequency and therefore to an increase of the effective propagation velocity $\omega/\langle k\rangle$. As in this example the background velocity is in the electron diamagnetic direction the propagation velocity in the plasma frame is also in the electron diamagnetic velocity (Eq. (1)).

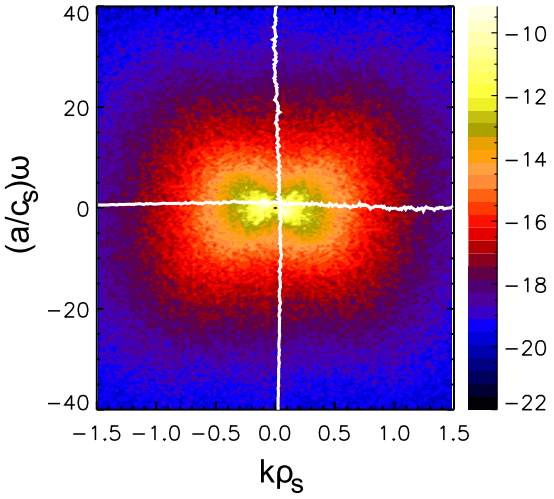

FIG. 12: Strong turbulence case: Wavenumber-frequency power spectrum $P(k,\omega)$ of density fluctuations at $\rho = 0.995$. Data is shown in the plasma frame of reference. Averaged frequencies and wavenumbers are shown by the white lines.

By mapping the wavenumber-frequency power spectrum $P(k,\omega)$ to the plasma frame $P(k,\omega - u_{E\times B}k)$ it has to be taken into account that in the present case the background velocity is time dependent $u_{E\times B}(t)$. Therefore, every sub time interval has to be mapped in the plasma frame and the ensemble average is done afterward. The wavenumber-frequency power spectrum $P(k,\omega)$in the plasma frame is shown in Fig. 12. It exhibits clear broadband characteristics. No signs of dispersion are observable. As in the present regime no eigenfrequency $\omega_l = \langle\omega\rangle - u_{E\times B}k$ is detectable, $\omega_l \ll \Delta\omega$. We have seen in Sec. IV that also the growth rate is negligible $\gamma \ll \Delta\omega$. Therefore, the presented regime is not only marginal but clearly in the strong turbulence regime $(\omega_l, \gamma_l \ll \Delta\omega)$.

A shift to low frequencies due to the nonlinear energy transfer as observed by the red line in Fig. 11a is not observed by the Doppler reflectometry [9–11] (Fig. 1b). By fitting a Gaussian the skewed part on the top of the spectrum which is the result of the cascade is basically ignored. In the average (Eq. (2)) the impact of this nonlinear shift is much stronger as the power is taken linearly and not logarithmicly into account. The resulting Doppler shift is shown by the black dotted line in Fig. 11a. The Doppler shift is more or less dispersionless and very close to the mean $E \times B$ velocity, which is basically in agreement with Refs.[9–11].

VI. DISCUSSION AND CONCLUSION

Plasma edge turbulence is characterized by high fluctuation levels. In particular the high level of small-scale vorticity fluctuations exhibiting strong shearing rates exceeding the growth rate by orders of magnitude [7] and are of comparable level to the eigenfrequencies of instabilities coming into consideration. Thereby linear features as growth rates and dispersion can be suppressed. This seems to be the reason of the vanishing phase velocity in the above shown typical case for ASDEX Upgrade L-mode discharges (Fig. 1). These small-scale vorticity fluctuations are generated by through nonlinear self-sustainment [6, 7, 29, 32]. It is important to note that the vorticity exhibits contribution from electrostatic potential and the ion pressure perturbations, where the later increases with the ion to electron temperature ratio which cannot be neglected in the plasma edge.

For even stronger turbulence measurements of the phase velocity could still provide finite values. The nonlinear spectral energy distribution can be observed in wavenumber-frequency space. Broadband plasma edge turbulence shows a power law behavior in wavenumber and frequency space which is a result of energy transfer mainly from high to low wavenumbers and frequencies. Some energy is also transferred in the other direction. This is the dual cascade characteristic for two-dimensional turbulence. Due to the shift of energy away from the line $\omega = u_{E\times B}k$ to low wavenumbers, the wavenumber averaged phase velocity $u(\omega) = \omega/\langle k\rangle$ will be in direction of the background velocity. As a result of the energy transfer to low frequencies in the lab frame, the frequency averaged phase velocity $u(k) = \langle\omega\rangle/k$ will

be in the opposite direction as the background velocity.

Only if the system is in the weak turbulence regime $\omega_l \gg \Delta\omega \sim \gamma_l$ the phase velocity can be used as an indicator for the underlying instability. This should be the case for core turbulence where the fluctuation level and hence $\langle\tilde{\Omega}\rangle_{rms}$ and $\Delta\omega$ are much lower. For high confinement regimes the fluctuation levels are lower, but the difference to L-mode is not as strong as the cases compared in the present study. This requires detailed investigations in the future. For example in H-mode quasi coherent modes with low frequency broadening [35] and in I-mode a weakly coherent mode with high frequency broadening [36, 37] are observed. In general it can be recommended to verify phase velocity measurements based on a frequency dependent technique with a wavenumber dependent technique and vice versa.

Acknowledgements

This work has been carried out within the framework of the EUROfusion Consortium and has received funding from the Euratom research and training programme 2014-2018 under grant agreement No 633053. The views and opinions expressed herein do not necessarily reflect those of the European Commission.

[1] B. B. Kadomtsev, *Plasma Turbulence* (Academic, New York, 1965).
[2] H. Doerk, F. Jenko, T. Görler, D. Told, and M. J. Pueschel, Phys. Plasmas **19**, 055907 (2012).
[3] A. B. Navarro, T. Happel, T. Görler, F. Jenko, J. Abiteboul, A. Bustos, H. Doerk, D. Told, and A. U. Team, Phys. Plasmas **22**, 042513 (2015).
[4] D. Hatch, D. Told, F. Jenko, H. Doerk, M. G. Dunne, E. Wolfrum, E. Viezzer, the ASDEX Upgrade Team, and M. J. Pueschel, Nucl. Fusion **55**, 063028 (2015).
[5] P. Manz, J. E. Boom, E. Wolfrum, G. Birkenmeier, I. G. J. Classen, N. C. Luhmann Jr., U. Stroth, and ASDEX Upgrade Team, Plasma Phys. & Controlled Fusion **56**, 035010 (2014).
[6] B. D. Scott, Phys. Rev. Lett. **65**, 3289 (1990).
[7] B. D. Scott, Phys. Fluids B: Plasma Phys. **4**, 2468 (1992).
[8] B. D. Scott, New J. Physics **4**, 52 (2002).
[9] G. D. Conway, J. Schirmer, S. Klenge, W. Suttrop, and E. Holzhauer, Plasma Phys. & Controlled Fusion **46**, 951 (2004).
[10] D. Prisiazhniuk, A. Krämer-Flecken, G. D. Conway, T. Happel, A. Lebschy, P. Manz, V. Nikolaeva, U. Stroth, and the ASDEX Upgrade Team, Plasma Phys. & Controlled Fusion **59**, 025013 (2016).
[11] M. Hirsch, E. Holzhauer, J. Baldzuhn, B. Kurzan, and B. D. Scott, Plasma Phys. & Controlled Fusion **43**, 1641 (2001).
[12] G. D. Conway, C. Angioni, R. Dux, F. Ryter, A. G. Peeters, J. Schirmer, C. Troester, C. R. Group, and the ASDEX Upgrade team, Nucl. Fusion **46**, S799 (2006).
[13] T. Happel, A. B. Navarro, G. D. Conway, C. Angioni, M. Bernert, M. Dunne, E. Fable, B. Geiger, T. Görler, F. Jenko, et al., Physics of Plasmas **22**, 032503 (2015).
[14] L. Vermare, P. Hennequin, . D. Grcan, C. Bourdelle, F. Clairet, X. Garbet, R. Sabot, and the Tore Supra Team, Physics of Plasmas **18**, 012306 (2011).
[15] G. I. Taylor, Proc. R. Soc. London Ser. **A164**, 476 (1938).
[16] C. C. Lin, Q. Appl. Maths. **10**, 295 (1953).
[17] J. M. Beall, Y. C. Kim, and E. J. Powers, J. Appl. Phys. **53**, 3933 (1982).
[18] F. Mink, E. Wolfrum, M. Maraschek, H. Zohm, L. Horvath, F. M. Laggner, P. Manz, E. Viezzer, U. Stroth, and the ASDEX Upgrade Team, Plasma Phys. & Controlled Fusion **58**, 125013 (2016).
[19] N. Fedorczak, P. Manz, S. C. Thakur, M. Xu, G. R. Tynan, G. S. Xu, and S. C. Liu, Phys. Plasmas **19**, 122302 (2012).
[20] L. M. Shao, G. S. Xu, S. C. Liu, S. J. Zweben, B. N. Wan, H. Y. Guo, A. D. Liu, R. Chen, B. Cao, W. Zhang, et al., Plasma Phys. & Controlled Fusion **55**, 105006 (2013).
[21] T. Kobayashi, G. Birkenmeier, E. Wolfrum, F. M. Laggner, M. Willensdorfer, U. Stroth, S. Inagaki, S.-I. Itoh, and K. Itoh, Rev. Sci. Inst. **85**, 083507 (2014).
[22] T. Munsat and S. J. Zweben, Rev. Sci. Inst. **77**, 103501 (2006).
[23] J. A. Krommes, Phys. Rep. **360**, 1 (2002).
[24] B. D. Scott, Contrib. Plasma Phys. **46**, 714 (2006).
[25] A. Kendl, B. D. Scott, and T. T. Ribeiro, Phys. Plasmas **17**, 072302 (2010).
[26] V. V. Bulanin and M. V. Yafanov, Plasma Phys. Rep. **32**, 47 (2006).
[27] T. Happel, E. Blanco, and T. Estrada, Rev. Sci. Inst. **81**, 10D901 (2010).
[28] G. D. Conway, B. Scott, J. Schirmer, M. Reich, A. Kendl, and the ASDEX Upgrade Team, Plasma Phys. & Controlled Fusion **47**, 1165 (2005).
[29] B. D. Scott, Phys. Plasmas **12**, 062314 (2005).
[30] S. J. Camargo, D. Biskamp, and B. D. Scott, Phys. Plasmas **2**, 48 (1995).
[31] P. Manz, M. Ramisch, and U. Stroth, Plasma Phys. & Controlled Fusion **51**, 035008 (2009).
[32] P. Manz, M. Xu, S. C. Thakur, and G. R. Tynan, Plasma Phys. & Controlled Fusion **53**, 095001 (2011).
[33] P. Manz, G. Birkenmeier, M. Ramisch, and U. Stroth, Phys. Plasmas **19**, 082318 (2012).
[34] R. H. Kraichnan, Phys. Fluids **10**, 1417 (1967).
[35] F. M. Laggner, E. Wolfrum, M. Cavedon, F. Mink, E. Viezzer, M. G. Dunne, P. Manz, H. Doerk, G. Birkenmeier, R. Fischer, et al., Plasma Phys. & Controlled Fusion **58**, 065005 (2016).
[36] I. Cziegler, P. H. Diamond, N. Fedorczak, P. Manz, G. R. Tynan, M. Xu, A. E. Hubbard, B. Lipschultz, J. M. Sierchio, J. L. Terry, et al., Phys. Plasmas **20**, 055904 (2013).
[37] P. Manz, P. Lauber, V. E. Nikolaeva, T. Happel, F. Ryter, G. Birkenmeier, A. Bogomolov, G. D. Conway, M. E. Manso, M. Maraschek, et al., Nucl. Fusion **55**, 083004 (2015).